Substrate recognition strategy for botulinum neurotoxin serotype A

Mark A. Breidenbach[1] **& Axel T. Brunger**[2]

[1]*Department of Molecular and Cellular Physiology and* [2]*Howard Hughes Medical Institute and Departments of Molecular and Cellular Physiology, Neurology and Neurological Sciences and Stanford Synchrotron Radiation Laboratory, Stanford University, Stanford, California 94305, USA*

Clostridal neurotoxins (CNTs) are the causative agents of the neuroparalytic diseases botulism and tetanus[1,2]. CNTs impair neuronal exocytosis through specific proteolysis of essential proteins called SNAREs[3]. SNARE assembly into a low-energy ternary complex is believed to catalyse membrane fusion, precipitating neurotransmitter release; this process is attenuated in response to SNARE proteolysis[4–7]. Site-specific SNARE hydrolysis is catalysed by the CNT light chains, a unique group of zinc-dependent endopeptidases[3]. The means by which a CNT properly identifies and cleaves its target SNARE has been a subject of much speculation; it is thought to use one or more regions of enzyme–substrate interaction remote from the active site (exosites)[8–10]. Here we report the first structure of a CNT endopeptidase in complex with its target SNARE at a resolution of 2.1 Å: botulinum neurotoxin serotype A (BoNT/A) protease bound to human SNAP-25. The structure, together with enzyme kinetic data, reveals an array of exosites that determine substrate specificity. Substrate orientation is similar to that of the general zinc-dependent metalloprotease thermolysin[11]. We observe significant structural changes near the toxin's catalytic pocket upon substrate binding, probably serving to render the protease competent for catalysis. The novel structures of the substrate-recognition exosites could be used for designing inhibitors specific to BoNT/A.

The structures of three CNT light chains suggest that substrate recognition cannot occur at the active sites of these proteases because the catalytic pocket composition and geometries of BoNTs A, B and E are essentially identical[12–14] (Fig. 1). Furthermore (and atypically for endopeptidases), light-chain activity can be strongly influenced by remote substitutions and deletions[10,15,16]. For example, conserved motifs containing acidic residues in the substrates were shown to be required for normal levels of light-chain activity and led to the proposal that the light chains may use exosites for efficient substrate recognition and cleavage[8–10,17]. However, structural data concerning the locations and functions of these exosites have remained elusive until now.

We created an inactive variant of BoNT/A light chain, because attempts to co-crystallize the wild-type BoNT/A light chain failed. Although a single-point mutation (E224Q) substantially impaired substrate turnover as previously observed[18], we detected cleavage products at the high concentrations of enzyme required for crystallization. A second mutation known to impair catalysis, Y366F, was added to eliminate substrate turnover at the conditions required for crystallization[19]. As a control, the double-mutant apo structure was solved by molecular replacement to 2.2 Å resolution (see Supplementary Methods) and found to be essentially identical to the wild-type structure[12], including side-chain orientations at positions 224 and 366 (Fig. 1). The carboxy-terminal SNARE (soluble N-ethylmaleimide-sensitive factor attachment protein receptor) domain of synaptosome-associated protein-25 kDa (SNAP-25), residues 141–204 (referred to as sn2), was co-crystallized with the double mutant BoNT/A light chain, and the structure of the complex was solved by molecular replacement to 2.1 Å resolution (see Supplementary Methods). Electron density for nearly all of sn2 (residues 146–204) was observed and independently confirmed by experimental anomalous sulphur phasing. The interface between the endopeptidase and substrate is extensive, wrapping around most of the light chain's circumference (Fig. 2). The interface buries approximately 4,840 Å^2 of surface area, about three times the area observed in thrombin–inhibitor complexes[20]. In contrast to the contiguous helical conformation of sn2 within the ternary SNARE core complex[21], sn2 adopts three distinct types of secondary structure in complex with BoNT/A: residues 147–167 form a distorted α-helix, residues 168–200 are extended and residues 201–204 are involved in a distorted β-sheet conformation. The observed interface between BoNT/A and sn2 is consistent with the previous report of a truncated substrate that is cut with the same efficiency as full-length SNAP-25 (ref. 15). The validity of a previously reported BoNT/B–SNARE complex[13] has been questioned[22], primarily owing to the absence of observed electron density for the substrate (see Supplementary Fig. 2). The reported BoNT/B–SNARE complex also features highly improbable ligand stereochemistry and provides little insight regarding determinants of substrate specificity, making our sn2–BoNT/A complex the first credible structure of a substrate-bound CNT light chain.

The amino-terminal helical region of sn2 interacts with the endopeptidase along a hydrophobic patch formed at the interface of four light-chain α-helices, referred to as the α-exosite (Figs 2, 3a): residues 102–113 (α-helix 1), 310–321 (α-helix 2), 335–348 (α-helix 3), and 351–358 (α-helix 4). The hydrophilic face of the amphipathic sn2 helix is oriented towards the solvent, while the hydrophobic side chains are buried against the α-exosite. Mutations to hydrophobic sn2 residues at this interface, including I156E and M167E, substantially decrease k_{cat}/K_m ratios (catalytic efficiency) compared to wild-type sn2 by increasing K_m (the Michaelis constant) (Fig. 4). N-terminally truncated substrates incapable of binding the α-exosite exhibit a further reduction in k_{cat}/K_m; the reported K_m for SNAP-25 residues 187–203 is ~55 times greater than that for SNAP-25 residues 1–206, whereas reported k_{cat} (turnover rate) values for these substrates are identical within

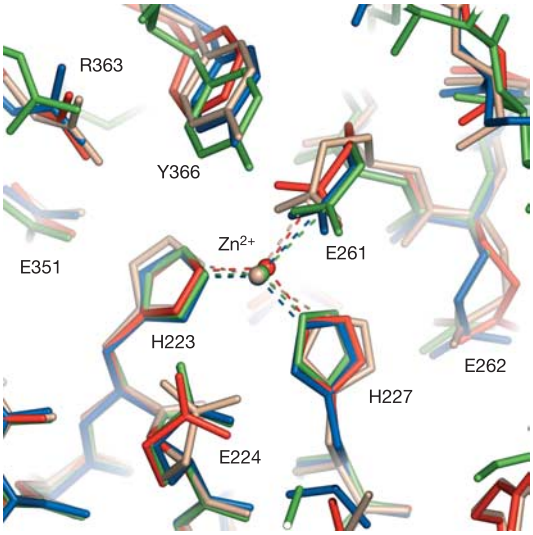

Figure 1 The nearly identical active sites of different BoNT light chains. The superimposed catalytic pockets of BoNT/A (tan), the E224Q/Y366F mutant of apo BoNT/A (red), BoNT/B (blue), and BoNT/E (green), with target sites $P_4P_3P_2P_1/P_1'P_2'P_3'P_4'$ (that is, the residue positions upstream and downstream of the protease cleavage site) Glu-Ala-Asn-Gln/Arg-Ala-Thr-Lys (BoNT/A), Gly-Ala-Ser-Gln/Phe-Glu-Thr-Ser (BoNT/B) and Gln-Ile-Asp-Arg/Ile-Met-Glu-Lys (BoNT/E) shown with BoNT/A residue numbering. Coordinates for wild-type BoNT/A, BoNT/B, and BoNT/E are from the Protein Data Bank (accession codes 3BTA, 1F82, 1T3A)[12–14]. Notably, the structure of the E224Q/Y366F mutant of BoNT/A is similar to that of wild-type BoNT/A. The fourth ligand of Zn^{2+} is a water molecule coordinated by Glu 224; for clarity it is not shown.

the margins of error[18,23,24]. Interestingly, conserved acidic residues of sn2 including Asp 147, Glu 148, and Glu 151 do not directly contact BoNT/A. Similar groups of charged residues have been implicated in mediating light chain–SNARE interactions in BoNTs B, G and tetanus neurotoxin, suggesting that SNARE recognition sites differ among the light chains[9]. Notably, the α-exosite of the BoNT/A light chain is structurally distinct from the hydrophobic interface formed in the ternary SNARE core complex[21] that binds the same stretch of sn2.

In the BoNT/A light chain–sn2 complex, the C-terminal portion of sn2 forms one strand of a distorted, three-stranded antiparallel β-sheet in a region that we refer to as the β-exosite (Figs 2, 3b, 5). This is the first example of β-sheet conformation observed in any SNARE protein, and further illustrates the conformational variability of SNAREs[25]. The other two strands of the β-sheet are contributed by the '250 loop' of the light chain, a region encompassing residues 242–259 (Figs 2, 3b). Specifically, residues 252–257 of the central strand pair with sn2 residues 201–204. The β-exosite interface is primarily mediated by backbone interactions, with the exception of Met 202 of sn2. Met 202 packs into a hydrophobic cavity formed by the interface of the light-chain 250 loop and the '370 loop', a region that encompasses light-chain residues 359–370. The 370 loop protrudes into the active site (Figs 2, 5) and separates the 250 loop from the catalytic pocket. Kinetic data linking the β-exosite (including the 370 loop and the C terminus of the substrate) to k_{cat} are available: the BoNT/A Y366F and R363A mutations are known to reduce k_{cat} ~40-fold and ~80-fold respectively, but K_m values remain nearly identical to the wild type[19]. Our kinetic characterization of the sn2 mutant M202Y revealed that the increased K_m of this mutant substrate was offset by an increase in k_{cat}, providing further evidence that structural changes in the β-exosite can directly influence k_{cat} (Fig. 4). Notably, substrates with C-terminal truncations at residue positions lower than Met 202 cannot be cut by BoNT/A at a measurable rate[24].

Connecting the α- and β-exosites, the extended portion of sn2 is channelled around the BoNT/A surface, leading directly through the catalytic pocket (Fig. 2). A small portion of the sn2 chain (residues 183–190) detaches from the surface of the light chain, rejoining the endopeptidase at sn2 residue Arg 191 and leading directly into the active site. Substrate electron density in the catalytic pocket (from sn2 residues 197–199) is fragmented, probably owing to the BoNT/A Y366F mutation, which might prevent a critical enzyme–substrate contact. Electron density is sufficient, however, to show a sharp, stereochemically strained turn leading out of the active site and connecting directly to the β-exosite (Fig. 5).

Several residues in the extended portion of sn2 are involved in side chain–side chain contacts with the endopeptidase at a series of anchor points that could serve as additional determinants of substrate specificity (Fig. 2, Supplementary Fig. 1). Substrate residues 170–172 and 192–193 comprise two distinct, contiguous anchor points, and individual side chains from Arg 176, Ile 178, Ile 181 and Glu 183 are also recognized by the endopeptidase. These anchor points, accounting for nearly half of the side chain–side chain contacts, assist in directing the path of the substrate into the endopeptidase's active site and can be classified as additional exosites (see Supplementary Fig. 1).

The availability of multiple apo crystal structures[12,26] along with our structure of the complex allowed us to discriminate between conformational changes resulting from crystal contacts, substrate binding and point mutations. Along the interface spanning from the α-exosite to the catalytic pocket, we observe only minor side-chain rearrangements in the light chain. The largest structural changes that are related to sn2 binding occur in the 250 loop and 370 loop at the β-exosite (Fig. 5). In apo BoNT/A, the 250 loop adopts an open conformation which contracts and folds over the 370 loop upon sn2 binding at the β-exosite (Fig. 5). Bulky side chains from both sn2 and the 250 loop including Met 202 and Tyr 250, respectively, pack against a stretch of the 370 loop and also influence its conformation.

Additional changes stem from the interaction of the Y366F

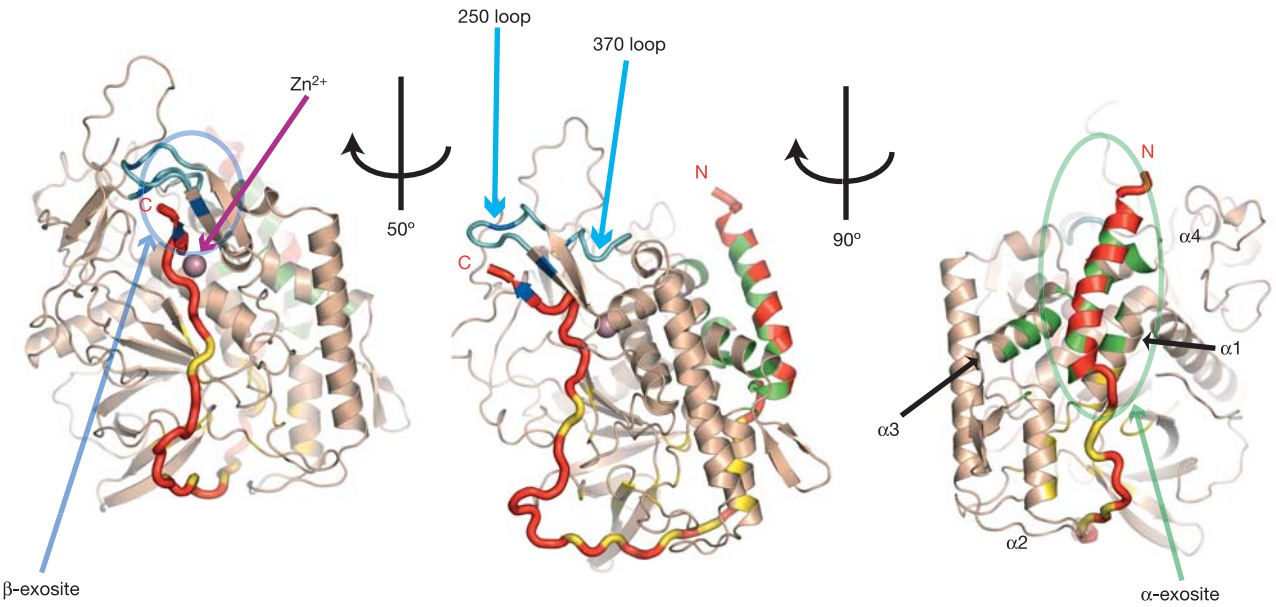

Figure 2 The interface between sn2 and BoNT/A. Three different views of the sn2–BoNT/A complex are shown; these are related by the specified rotations around a vertical axis in the plane of the figure that goes through the centre of the complex. The α-exosite (indicated by a green arrow) is formed by BoNT/A light-chain helices (tan) α1–α4 that bind to the helical N terminus of sn2 (red). Green areas indicate the approximate locations of contacting side chains involved in the α-exosite. On the opposite face of sn2–BoNT/A, the β-exosite is indicated by a blue arrow. The C terminus of sn2 forms an anti-parallel β sheet along with a portion of the 250 loop (light-blue), which is separated from the active site (indicated by Zn^{2+}, purple sphere) by the 370 loop (light-blue). Dark-blue areas indicate the approximate location of contacting side chains involved in the β-exosite. Yellow areas indicate the approximate location of other residues (anchor points) involved in side-chain contacts between the sn2 substrate and the BoNT/A light chain. A detailed list of all contacts between sn2 and BoNT/A light chain can be found in Supplementary Fig. 1.

mutation with sn2. Incapable of forming a hydrogen bond with the substrate, the mutant Phe 366 residue is reoriented to point away from sn2 (Figs 1, 5). The new Phe 366 position causes a cascade of additional side-chain reorientations, leading to salt-bridge formation between Arg 363 and Asp 370 (Fig. 5). This salt bridge buttresses the entire 370 loop. We speculate that in wild-type BoNT/A, Tyr 366 would not be redirected away from Arg 198 and the salt bridge between Arg 363 and Asp 370 would not form.

BoNT/A shares the same His-Glu-X-X-His zinc-binding motif as thermolysin[12,19]. Our structure reveals that the directionality of the substrate is the same as that of peptide inhibitors bound to thermolysin[11] and that the positions of the primary catalytic residues match those found in thermolysin (see Supplementary Fig. 3). The scissile peptide bond of sn2, between Gln 197 and Arg 198, is positioned near the catalytic water molecule that is coordinated by Zn^{2+} (Fig. 5). Consistent with this model, the BoNT/A E224Q mutant no longer efficiently deprotonates the intervening water molecule. However, there are no obvious residues similar to thermolysin Tyr 157 and His 231, which have been proposed to stabilize the transition state[27]. In fact, the space occupied by these two residues in thermolysin is occupied by sn2 residues in the case of BoNT/A. Thus, it is possible that there are no specific residues to stabilize the evolving oxyanion, or that BoNT/A activity might involve substrate-assisted catalysis[28], where polar groups at the sharp kink following the scissile bond (such as the side-chain hydroxyl or backbone amide of Thr 200) could stabilize the transition state.

Interestingly, a homodimeric structure of BoNT/A shows an interaction between a C-terminal fragment of the autolysed 250

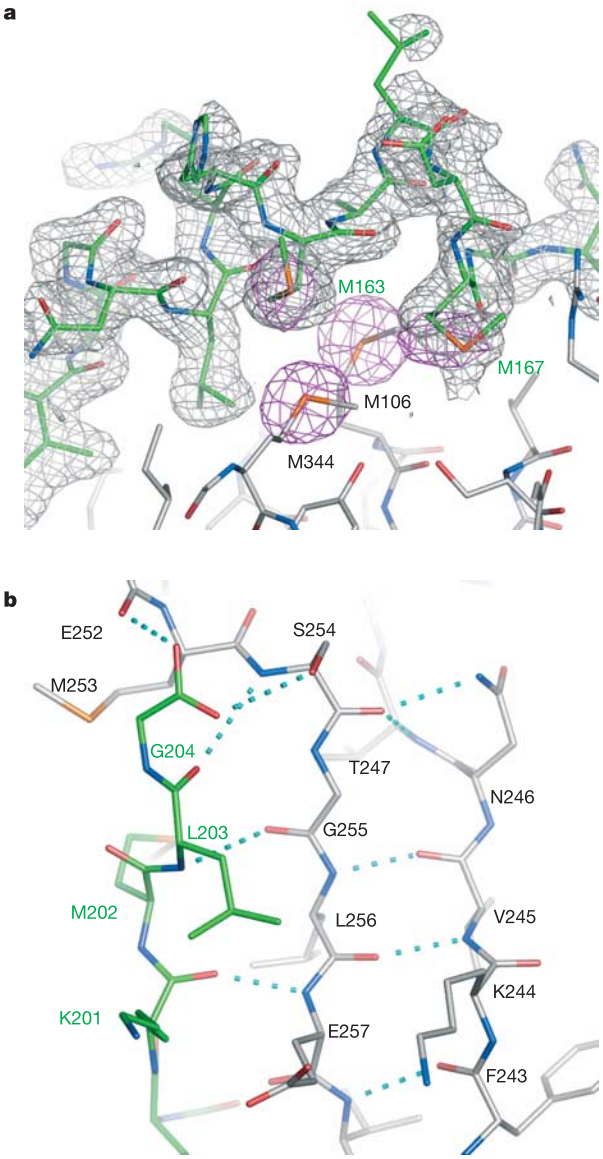

Figure 3 Detailed views of α- and β-exosites. **a**, A cross-validated, σ_A-weighted, phase-combined ($2m|F_o|\phi_{comb} - D|F_c|\phi_{calc}$, where ϕ_{comb} and ϕ_{calc} are the combined and model phases, respectively, m is the combined figure of merit and D is an estimate of the model's completeness, both obtained from the σ_A method) spherical OMIT map with simulated annealing is shown, centred on Met 163 and contoured at 1σ (grey mesh). Anomalous Fourier difference density (violet mesh) contoured at 4σ highlights sulphur atoms in sn2 and nearby BoNT/A methionine (M) residues. **b**, The β-sheet network of hydrogen bonds (cyan dashes) between the 250 loop (grey backbone) and sn2 (green backbone) is shown.

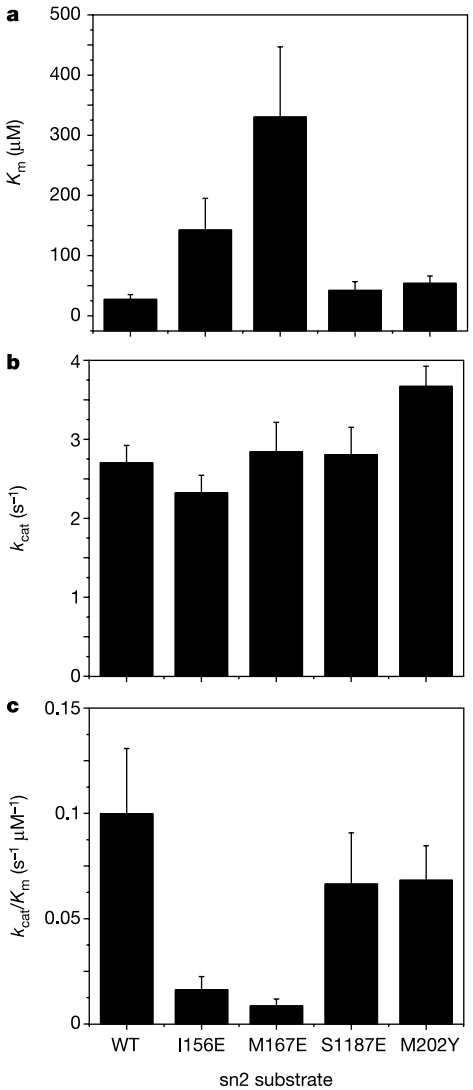

Figure 4 Kinetic characterization of sn2 mutants. Kinetic analyses (see Supplementary Methods) were conducted for mutant substrates that were designed to disrupt hydrophobic packing observed at the α- and β-exosites. S187E serves as a negative control because it makes no contacts with the light chain in our structure. **a**, K_m values for wild-type (WT) and mutant substrates. **b**, Values for k_{cat} for wild-type and mutant substrates. **c**, The ratio k_{cat}/K_m for each substrate. Error bars represent estimates of s.e.m. Kinetic parameters obtained using the wild-type sn2 substrate are consistent with previously reported results[18].

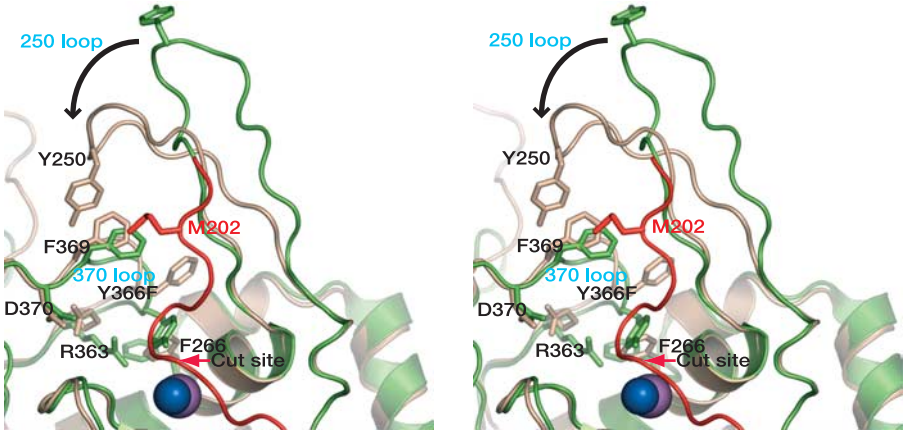

Figure 5 Wall-eyed stereo view of β-exosite conformational changes. The 250 loop switches from an open (green) to a closed (tan) conformation upon sn2 (red) binding. With substrate bound, the 250 loop packs against the 370 loop, which borders the catalytic pocket. The scissile bond (indicated by red arrow) is suspended above the nucleophilic water (blue sphere), shown coordinated by Zn^{2+} (purple sphere) in the active site. Distortion of the 370 loop is restricted by a salt bridge between Arg 363 and Asp 370. A void caused by the reorientation of the mutant Phe 366 is filled by Phe 266, displacing the Arg 363 side chain. In wild-type BoNT/A, we speculate that deformation of a more dynamic 370 loop could place the acyl carbon of Gln 197 within range of the attacking nucleophile.

loop of one monomer with the active site of the other BoNT/A monomer[26]. However, the C terminus has the opposite (non-canonical) orientation compared to our structure and thermolysin. This structure probably does not represent a physiologically relevant product-bound configuration of the native substrate. We note that BoNT/A is able to cleave non-specific substrates (such as the 250 loop from another BoNT/A monomer) in the non-canonical orientation, but this occurrence seems to be restricted to the conditions of low pH (4.6) and high protein concentration used in the crystallization of this complex. As mentioned above, a purported product-bound BoNT/B structure[13] has been shown to be an artefact of model bias[22] (see Supplementary Fig. 2).

Based on our structure and available kinetic data for several SNAP-25 substrates, a general model of the strategy used by BoNT/A to recognize and cleave SNAP-25 is presented in Fig. 6a–c. With a full-length substrate, sn2 helix induction can occur at the α-exosite, orienting the peptide to assist in the formation of anchor points along the extended substrate chain (Fig. 6b). BoNT/A can cleave small peptides (sn2 residues 192–206) capable of binding only one anchor point in addition to the β-exosite, but only with a substantial reduction in k_{cat}/K_m (refs 18, 23, 24). The absence of a conformational change in BoNT/A upon binding to the α-exosite and anchor points is consistent with unchanged k_{cat} values for full-length and N-terminally truncated peptides, as well as our I156E and M167E point mutants. Thus, most of the enzyme–substrate interface serves to provide a substrate-specific boost to k_{cat}/K_m by reducing K_m. The entropic penalty of orienting an otherwise unstructured polypeptide chain[25,29] into the observed complex may be largely offset in a substrate-specific manner by the unusually large number of substrate–enzyme contacts at the exosites. Although the β-exosite itself does not confer much substrate specificity, its presence is vital for activity[24] and it probably serves to activate the endopeptidase via its contacts with the 370 loop. Our structure also explains the inability of BoNT/A to cleave SNAP-25 when it is present as a complex with other SNAREs (Fig. 6d), because the complexed sn2 is restricted to an entirely helical conformation.

The locations and compositions of the exosites are likely to vary between different BoNT light chains. The α-exosite used by BoNT/A is not conserved on the surface of BoNT/E, which also cuts the same sn2 substrate albeit at a different position. The placement of the exosites may be the primary determinants of scissile bond location and might account for the 17-residue shift in cleavage sites between BoNT/A and BoNT/E. Our structural description of the critical exosites on the surface of BoNT/A that recognize sn2 may lead to development of highly specific inhibitors for this neurotoxin. In particular, the α-exosite could be a candidate for structure-based design using a strategy similar to that used in the successful

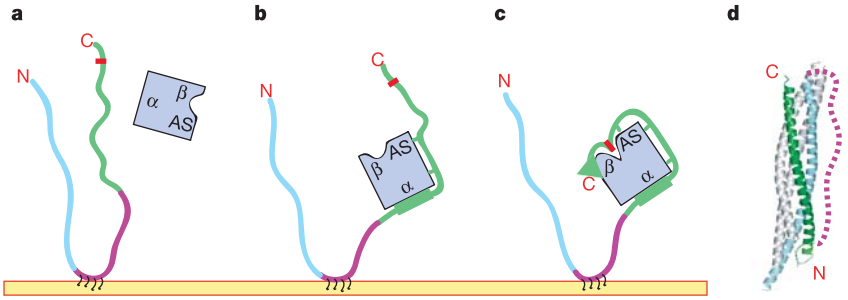

Figure 6 Exosite-based model of BoNT/A substrate recognition. **a**, SNAP-25 is shown attached to a presynaptic membrane via palmitylation sites (shown in black) on its linker domain (purple). The N-terminal (sn1, cyan) and C-terminal (sn2, green) domains are unstructured or flexible in uncomplexed SNAP-25 (ref. 29). **b**, Binding of BoNT/A (blue) is probably initiated by helix formation at the α-exosite, and anchor points along the extended portion of SNAP-25 (green notches) are additional determinants of substrate specificity. **c**, These sites reduce K_m and enhance binding at the β-exosite, inducing conformational changes at the active site (AS) via the 370 loop, which render the endopeptidase competent to cleave its substrate. **d**, The sn2 domain of SNAP-25 (same colour scheme as in **a**–**c**) adopts a continuous helical conformation in the SNARE complex.

development of HIV-1 entry inhibitors based on the core structure of gp41 (ref. 30). □

Methods

Details and references are provided in the Supplementary Information which accompanies this paper. Briefly, recombinant apo BoNT/A E224Q/Y366F (residues 2–420) was crystallized by hanging-drop vapour diffusion against 15–18% PEG 3350 and 200 mM di-sodium hydrogen phosphate dihydrate at 20 °C. These crystals indexed in space group *P*2 with near-orthorhombic unit cell dimensions $a = 57.90$ Å, $b = 40.49$ Å, $c = 195.89$ Å and $\beta = 90.25°$. Co-crystallization of the complex was performed using a mixture of the inactive BoNT/A light chain with a molar excess of SNAP-25 (residues 141–204), equilibrated against 10% (w/v) PEG 8000, 200 mM magnesium acetate and 100 mM sodium cacodylate (pH 6.5) at 4 °C. These crystals indexed in space group $P4_32_12$ with unit cell dimensions $a = b = 86.0$ Å, $c = 165.4$ Å. All diffraction data were collected at the Advanced Light Source (beamlines 8.2.1 and 8.2.2) and at the Stanford Synchrotron Radiation Lab (beamline 9-2). The diffraction data were indexed and scaled with MOSFLM and SCALA in the CCP4 computational suite. Initial phases for both structures were obtained by molecular replacement (MR) using light chain coordinates from wild-type BoNT/A (Protein Data Bank accession code 3BTA). For the complex, experimental sulphur single-wavelength anomalous dispersion (SAD) phases were computed and used both as an independent confirmation of the sn2 trace and to supplement the MR phases. All phasing and refinement calculations were performed using the Crystallography and NMR System version 1.1 (CNS). The E224Q/Y366F apo BoNT/A structure was solved to 2.2 Å resolution with final $R_{working} = 22.0\%$ and $R_{free} = 27.3\%$, where $R_{working} = \Sigma_{hkl}|F_o - F_c|/\Sigma_{hkl}|F_o|$ (where F_o and F_c are the observed and model structure factor amplitudes, respectively) and R_{free} is equivalent to $R_{working}$ but is calculated for a randomly chosen 5% of reflections excluded from model refinement. The sn2–BoNT/A complex structure was determined to 2.1 Å with final $R_{working} = 21.9\%$ and $R_{free} = 24.9\%$. Structural illustrations were prepared using Pymol. Kinetic parameters were determined by quantifying C-terminal cleavage products of various sn2 substrates following partial digestion with wild-type BoNT/A light chain. Cleavage products were fractionated by reverse-phase high-performance liquid chromatography (RP-HPLC) on a 218TP54 column (Vydac), and plots of reaction velocity as a function of substrate concentration were fitted to the Michaelis-Menten equation to yield K_m, k_{cat} and error estimates.

Received 21 September; accepted 19 October 2004; doi:10.1038/nature03123.
Published online 12 December 2004.

1. Humeau, Y., Doussau, F., Grant, N. J. & Poulain, B. How botulinum and tetanus neurotoxins block neurotransmitter release. *Biochimie* **82,** 427–446 (2000).
2. Dolly, J. O., Black, J., Williams, R. S. & Melling, J. Acceptors for botulinum neurotoxin reside on motor nerve terminals and mediate its internalization. *Nature* **307,** 457–460 (1984).
3. Schiavo, G. *et al.* Tetanus and botulinum-B neurotoxins block neurotransmitter release by proteolytic cleavage of synaptobrevin. *Nature* **359,** 832–835 (1992).
4. Chen, Y. A., Scales, S. J., Patel, S. M., Doung, Y. C. & Scheller, R. H. SNARE complex formation is triggered by Ca^{2+} and drives membrane fusion. *Cell* **97,** 165–174 (1999).
5. Söllner, T. *et al.* SNAP receptors implicated in vesicle targeting and fusion. *Nature* **362,** 318–324 (1993).
6. Pellegrini, L. L., O'Connor, V., Lottspeich, F. & Betz, H. Clostridial neurotoxins compromise the stability of a low energy SNARE complex mediating NSF activation of synaptic vesicle fusion. *EMBO J.* **14,** 4705–4713 (1995).
7. Xu, T., Binz, T., Niemann, H. & Neher, E. Multiple kinetic components of exocytosis distinguished by neurotoxin sensitivity. *Nature Neurosci.* **1,** 192–200 (1998).
8. Rossetto, O. *et al.* SNARE motif and neurotoxins. *Nature* **372,** 415–416 (1994).
9. Pellizzari, R. *et al.* Structural determinants of the specificity for synaptic vesicle-associated membrane protein/synaptobrevin of tetanus and botulinum type B and G neurotoxins. *J. Biol. Chem.* **271,** 20353–20358 (1996).
10. Cornille, F. *et al.* Cooperative exosite-dependent cleavage of synaptobrevin by tetanus toxin light chain. *J. Biol. Chem.* **272,** 3459–3464 (1997).
11. Holden, H. M., Tronrud, D. E., Monzingo, A. F., Weaver, L. H. & Matthews, B. W. Slow- and fast-binding inhibitors of thermolysin display different modes of binding: crystallographic analysis of extended phosphonamidate transition-state analogues. *Biochemistry* **26,** 8542–8553 (1987).
12. Lacy, D. B., Tepp, W., Cohen, A. C., DasGupta, B. R. & Stevens, R. C. Crystal structure of botulinum neurotoxin type A and implications for toxicity. *Nature Struct. Biol.* **5,** 898–902 (1998).
13. Hanson, M. A. & Stevens, R. C. Cocrystal structure of synaptobrevin-II bound to botulinum neurotoxin type B at 2.0 Å resolution. *Nature Struct. Biol.* **7,** 687–692 (2000).
14. Agarwal, R., Eswaramoorthy, S., Kumaran, D., Binz, T. & Swaminathan, S. Structural analysis of botulinum neurotoxin type E catalytic domain and its mutant glu212 → gln reveals the pivotal role of the glu212 carboxylate in the catalytic pathway. *Biochemistry* **43,** 6637–6644 (2004).
15. Vaidyanathan, V. V. *et al.* Proteolysis of SNAP-25 isoforms by botulinum neurotoxin types A, C, and E: domains and amino acid residues controlling the formation of enzyme-substrate complexes and cleavage. *J. Neurochem.* **72,** 327–337 (1999).
16. Foran, P., Shone, C. C. & Dolly, J. O. Differences in the protease activities of tetanus and botulinum B toxins revealed by the cleavage of vesicle-associated membrane protein and various sized fragments. *Biochemistry* **33,** 15365–15374 (1994).
17. Washbourne, P., Pellizzari, R., Baldini, G., Wilson, M. C. & Montecucco, C. Botulinum neurotoxin types A and E require the SNARE motif in SNAP-25 for proteolysis. *FEBS Lett.* **418,** 1–5 (1997).
18. Li, L., Binz, T., Niemann, H. & Singh, B. R. Probing the mechanistic role of glutamate residue in the zinc-binding motif of type A botulinum neurotoxin light chain. *Biochemistry* **39,** 2399–2405 (2000).
19. Binz, T., Bade, S., Rummel, A., Kollewe, A. & Alves, J. Arg(362) and Tyr(365) of the botulinum neurotoxin type A light chain are involved in transition state stabilization. *Biochemistry* **41,** 1717–1723 (2002).
20. Brooijmans, N., Sharp, K. A. & Kuntz, I. D. Stability of macromolecular complexes. *Proteins* **48,** 645–653 (2002).
21. Sutton, R. B., Fasshauer, D., Jahn, R. & Brunger, A. T. Crystal structure of a SNARE complex involved in synaptic exocytosis at 2.4 Å resolution. *Nature* **395,** 347–353 (1998).
22. Rupp, B. & Segelke, B. Questions about the structure of the botulinum neurotoxin B light chain in complex with a target peptide. *Nature Struct. Biol.* **8,** 663–664 (2001).
23. Sukonpan, C. *et al.* Synthesis of substrates and inhibitors of botulinum neurotoxin type A metalloprotease. *J. Pept. Res.* **63,** 181–193 (2004).
24. Schmidt, J. J. & Bostian, K. A. Proteolysis of synthetic peptides by type A botulinum neurotoxin. *J. Protein Chem.* **14,** 703–708 (1995).
25. Fiebig, K. M., Rice, L. M., Pollock, E. & Brunger, A. T. Folding intermediates of SNARE complex assembly. *Nature Struct. Biol.* **6,** 117–123 (1999).
26. Segelke, B., Knapp, M., Kadkhodayan, S., Balhorn, R. & Rupp, B. Crystal structure of Clostridium botulinum neurotoxin protease in a product-bound state: evidence for noncanonical zinc protease activity. *Proc. Natl Acad. Sci. USA* **101,** 6888–6893 (2004).
27. Matthews, B. W. Structural basis of the action of thermolysin and related zinc peptidases. *Acc. Chem. Res.* **21,** 333–340 (1988).
28. Dall'Acqua, W. & Carter, P. Substrate-assisted catalysis: molecular basis and biological significance. *Protein Sci.* **9,** 1–9 (2000).
29. Fasshauer, D., Bruns, D., Shen, B., Jahn, R. & Brunger, A. T. A structural change occurs upon binding of syntaxin to SNAP-25. *J. Biol. Chem.* **272,** 4582–4590 (1997).
30. Debnath, A. K., Radigan, L. & Jiang, S. Structure-based identification of small molecule antiviral compounds targeted to the gp41 core structure of the human immunodeficiency virus type 1. *J. Med. Chem.* **42,** 3203–3209 (1999).

Supplementary Information accompanies the paper on **www.nature.com/nature**.

Acknowledgements We thank T. Binz and J. Ernst for providing initial BoNT/A and sn2 constructs and P. Adams, T. Fenn, S. Kaiser, Z. Panepucci, P. Strop and W. Weis for technical assistance and critical reading. Portions of this research were carried out at the Stanford Synchrotron Radiation Laboratory, a national user facility operated by Stanford University on behalf of the US Department of Energy (Office of Basic Energy Sciences). The SSRL Structural Molecular Biology Program is supported by the Department of Energy (Office of Biological and Environmental Research) and by the National Institutes of Health (National Center for Research Resources, Biomedical Technology Program) and the National Institute of General Medical Sciences. Portions of this research were conducted at the Advanced Light Source which is supported by the Office of Energy Research (Office of Basic Energy Sciences, Materials Sciences Division) of the US Department of Energy at Lawrence Berkeley National Laboratory. This work was supported in part by an NIH grant to A.T.B.

Competing interests statement The authors declare that they have no competing financial interests.

Correspondence and requests for materials should be addressed to A.T.B. (brunger@stanford.edu). The coordinates and structure factors have been deposited in the Protein Data Bank under the accession codes 1XTF (apo structure) and 1XTG (complex).